AIAA JOURNAL
Vol. 30, No. 9, September 1992

Nonlinear Instability of Corrugated Diaphragms

Kai-yuan Yeh*
University of Toronto, Toronto, Ontario M5S 1A4, Canada
Wei-ping Song†
Lanzhou University, Lanzhou, Gansu 730 000, People's Republic of China
and
F. P. J. Rimrott‡
University of Toronto, Toronto, Ontario M5S 1A4, Canada

In this paper, the authors propose a method of solution to a set of nonlinear equations governing large axisymmetric deformation of shallow shells of revolution and study the deformations, stresses, and instability of circular corrugated diaphragms. The method is based on the integral equation method, the Newtonian iterative scheme, and spline approximation, and it is found that results have good convergence, such that they can be used for practical problems, and that they are readily programmed. By using this method, a set of equations for a circular corrugated diaphragms with sine-shaped shallow waves under normal pressure is solved. The displacements, stresses, and instability of the diaphragms are numerically analyzed in detail. The results show that corrugated diaphragms snap through several times, a characteristic that can be used as a design parameter of the element. The idea that the corrugated diaphragm can be used not only as a sensor but also as a control element is suggested by the authors of this paper.

Nomenclature

D = flexural rigidity
E = Young's modulus
$f(x)$ = free term
G_1, G_2 = Green functions
H = wave amplitude
h = thickness of the corrugated diaphragm
l = wave length
M_r = radial bending moment
M_θ = circumferential bending moment
N_r = radial membrane force per unit length
N_θ = circumferential membrane force per unit length
p = reduced load intensity, $r_1^4\sqrt{[12(1-\nu^2)]^3}q/2Eh^4$
p_{b1}, p_{b2}, p_{b3} = snap-back loads
p_{c1}, p_{c2}, p_{c3} = snap-through loads
Q_r = radial shearing force
Q_θ = circumferential shearing force
q = intensity of the uniform pressure acting on the corrugated diaphragm
r = radial coordinate
r_1 = radius of the corrugated diaphragm
r_2 = radius of the central plate of the corrugated diaphragm
U = reduced radial displacement, $12r_1(1-\nu^2)u/h^2$
u = radial displacement
W = reduced deflection, $\sqrt{12(1-\nu^2)}w/h$
w = deflection of the neutral surface of the thin shell
w_I = initial deflection of the neutral surface of the thin shell
x = reduced radial coordinate, r/r_1
x^* = ratio of radii, r_2/r_1
Y = reduced deflection that contains the initial deflection, $\sqrt{12(1-\nu^2)}(w+w_I)/h$
$\alpha(x)$ = reduced slope, $\sqrt{12(1-\nu^2)}(r_1/h)\,dw/dr$
$\beta(x)$ = reduced derivative of stress function, $[12(1-\nu^2)/Er_1]\,(r_1/h)\,d\Phi/dr$
δ_1, δ_2 = coefficients determined by different boundary conditions
Φ = stress function
λ = reduced wave amplitude, $\sqrt{12(1-\nu^2)}(r_1/h)\,2\pi H/l$
ν = Poisson's ratio
σ = stress
$\bar{\sigma}$ = reduced stress
σ_r = radial total stress
σ_r^b = radial bending stress
$\bar{\sigma}_r^b$ = reduced radial bending stress
σ_r^m = radial membrane stress
σ_θ = circumferential total stress
σ_θ^b = circumferential bending stress
$\bar{\sigma}_\theta^b$ = reduced circumferential bending stress
σ_θ^m = circumferential membrane stress
$\bar{\sigma}_\theta^m$ = reduced circumferential membrane stress
$\bar{\sigma}^m$ = reduced radial membrane stress
ϕ = phase angle
ω = reduced angular frequency, $2\pi r_1/l$

I. Introduction

CIRCULAR corrugated diaphragms have many technical applications. They have been, in particular, adopted widely as a low pressure sensor in precision instruments, meters, and transducers. Since Hersey[1] and Griffith[2] first studied the theory and performed the experiment on circular corrugated diaphragms, many researchers[3-19] have worked on the problem. Among them, Panov[3] was the first to discuss the large deflection problem of a circular corrugated diaphragm, and Haringx[4] first suggested the idea of reducing a corrugated diaphragm to an equivalent orthotropic plate. These studies increased our understanding of the behavior of corrugated diaphragms. However, as far as we know, many problems such as instability, deformation, and stress distribution in the case of large deflection of the corrugated diaphragm have not been well solved yet due to the complexity of their configura-

Received Jan. 29, 1991; revision received Dec. 5, 1991; accepted for publication Dec. 20, 1991.

*Visiting Professor, Department of Mechanical Engineering, 5 King's College Road.
†Associate Professor, Department of Mechanics.
‡Professor, Department of Mechanical Engineering, 5 King's College Road.

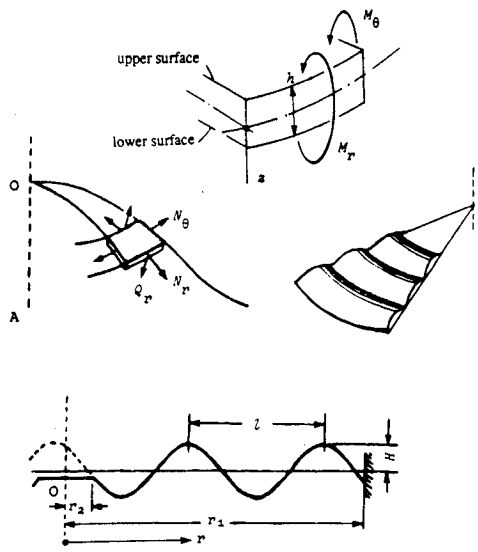

Fig. 1 Dimensions of the corrugated diaphragm shells and a shell element subjected to internal forces and moments.

tion on the one hand and inadequate methods of solution on the other.

The purpose of this paper is to present a method of solution—the Newton-spline method—to the nonlinear boundary-value problems governing the large axisymmetric deflection of shallow shells of revolution and study the deformations, stress, and instability of a circular corrugated diaphragm with sine-shaped shallow waves under normal pressure. As we know, there were many solutions[20-22] to the nonlinear problems for shells of revolution. These solutions are based either on Piccard iteration, which has poor rate of convergence, combined with a finite difference scheme or on Newtonian iteration combined with a finite difference scheme to the set of nonlinear equations of the shells, which contains at least two main unknown functions. The present method of solution is based on using the Newtonian iterative scheme and spline approximation to a nonlinear integral equation with only one unknown function, and hence, it not only has the quadratic rate of convergence of the Newtonian iterative procedure but also requires less computation and has fewer computation errors. Because the equivalent orthotropic plate theory cannot carry out the stress and buckling analyses of a corrugated diaphragm, the nonlinear equations of shallow shells of revolution of the von Kármán type are used here. It has been pointed out that these equations are not correct, as compared with Reissner's equations, for the reason that, in the equations of moment equilibrium and membrane force equilibrium for elements of shells, the influence of deformation is neglected. For practical purpose, however, the solutions of the von Kármán type equations are sufficiently good approximations for axisymmetric nonlinear bending of shells of revolution as pointed out in Ref. 22, and the equations are more convenient to be analysed than those of Reissner's.

II. Fundamental Equations

From the equations of rotational shallow shells given by Volmir,[8] we can derive the nonlinear deflection equations of a circular corrugated diaphragm with shallow sine-shaped waves under uniform pressure, as shown in Figure 1.

$$D\frac{d}{dr}\frac{1}{r}\frac{d}{dr}r\frac{dw}{dr}-\frac{h}{r}\frac{d\Phi}{dr}\left[\frac{dw}{dr}-\frac{2\pi H}{l}I(r-r_2)\sin\left(\frac{2\pi}{l}r+\phi\right)\right]=\frac{1}{2}qr \tag{1}$$

$$\frac{1}{E}\frac{d}{dr}\frac{1}{r}\frac{d}{dr}r\frac{d\Phi}{dr}+\frac{1}{r}\frac{dw}{dr}\left[\frac{1}{2}\frac{dw}{dr}+\frac{2\pi H}{l}I(r-r_2)\sin\left(\frac{2\pi}{l}r+\phi\right)\right]=0 \tag{2}$$

The term $I(r-r_2)$ is a Heaviside function defined as follows

$$I(r-r_2)=\begin{cases}1 & \text{as } r\geq r_2\\ 0 & \text{as } r<r_2\end{cases}$$

The boundary conditions are

At $r=r_1$:

$$w=0,\qquad \delta_1\frac{d^2w}{dr^2}+\frac{1}{r}\frac{dw}{dr}=0,\qquad \delta_2\frac{d^2\Phi}{dr}-\frac{1}{r}\frac{d\Phi}{dr}=0 \tag{3}$$

At $r=0$:

$$\frac{dw}{dr}=0,\qquad \frac{d\Phi}{dr}=0 \tag{4}$$

1) Edge simply supported ($r=r_1$, $w=0$, $M_r=0$, $N_r=0$):

$$\delta_1=\frac{1}{\nu},\qquad \delta_2=0$$

2) Edge simply hinged ($r=r_1$, $w=0$, $M_r=0$, $u=0$):

$$\delta_1=\frac{1}{\nu},\qquad \delta_2=\frac{1}{\nu}$$

3) Edge rigidly clamped ($r=r_1$, $w=0$, $dw/dr=0$, $u=0$):

$$\delta_1=0,\qquad \delta_2=\frac{1}{\nu},\ b_p$$

4) Edge clamped but free to slip ($r=r_1$, $w=0$, $dw/dr=0$, $N_r=0$):

$$\delta_1=\delta_2=0$$

Other values of δ_1 and δ_2, corresponding to various elastic support conditions, can also be determined.

After finding the deflection $w(r)$ and the stress function $\Phi(r)$, the bending moment, shearing force, membrane force per unit length, and radial horizontal displacement of the corrugated diaphragm can be determined by the following formulas:

$$M_r=-D\left(\frac{d^2w}{dr^2}+\frac{\nu}{r}\frac{dw}{dr}\right),\qquad M_\theta=-D\left(\frac{1}{r}\frac{dw}{dr}+\nu\frac{d^2w}{dr^2}\right)$$

$$Q_r=-D\frac{d}{dr}\frac{1}{r}\frac{d}{dr}r\frac{dw}{dr},\qquad N_r=\frac{h}{r}\frac{d\Phi}{dr},\qquad N_\theta=h\frac{d^2\Phi}{dr^2} \tag{5}$$

$$u=\frac{1}{E}\left(\frac{d^2\Phi}{dr^2}-\frac{\nu}{r}\frac{d\Phi}{dr}\right)$$

In order to simplify the fundamental equations and boundary conditions, let us introduce the following dimensionless variables

$$x=\frac{r}{r_1},\qquad \alpha(x)=\sqrt{12(1-\nu^2)}\frac{r_1}{h}\frac{dw}{dr}$$

$$\beta(x)=12(1-\nu^2)\left(\frac{r_1}{h}\right)^2\frac{d\Phi}{dr},\qquad \omega=2\pi\frac{r_1}{l} \tag{6}$$

$$\lambda=\sqrt{12(1-\nu^2)}\frac{r_1}{h}\frac{2\pi H}{l},\qquad x^*=\frac{r_2}{r_1},\qquad p=\frac{r_1^4\sqrt{[12(1-\nu^2)]^3}q}{2Eh^4}$$

Making use of Green functions, we can replace the boundary-value problem [Eqs. (1-4)] of the nonlinear differential equations (1) and (2) by an equivalent integral equation in dimensionless form

$$\alpha(x) + \int_0^1\int_0^1 G_1(x,s)\, G_2(s,t)\, [\alpha(s) + I(s - x^*)\lambda \sin(\omega s + \phi)]\, [\tfrac{1}{2}\alpha(t)^2 + I(t - x^*)\lambda \sin(\omega t + \phi)\alpha(t)]\, ds\, dt = -pf(x) \qquad (0 \le x \le 1) \qquad (7a)$$

$$\beta(x) = \int_0^1 G_2(x,s)\alpha(s)[\tfrac{1}{2}\alpha(s)^2 + I(s - x^*)\lambda \sin(\omega s + \phi)]\, ds \qquad (7b)$$

where Green functions G_1 and G_2 as well as the free term $f(x)$ are known functions on the square $0 \le x,\ s \le 1$, $0 \le s,\ t \le 1$, and interval $0 \le x \le 1$, respectively,

$$G_i(x,s) = \begin{cases} \tfrac{1}{2}[u_i s + (1/s)]x, & 0 \le x \le s \\ \tfrac{1}{2}[u_i x + (1/x)]s, & s \le x \le 1 \end{cases} \qquad (i = 1,2) \qquad (8)$$

$$u_1 = \frac{\delta_1 - 1}{\delta_1 + 1}, \qquad u_2 = \frac{\delta_2 + 1}{\delta_2 - 1} \qquad (9)$$

$$f(x) = -\frac{1}{8}\left(x^3 - \frac{3\delta_1 + 1}{\delta_1 + 1}\, x\right) \qquad (10)$$

The numerical programs used to solve integral equation (7) under boundary conditions (3) and (4) can be found in detail in Refs. 24 and 25. Here we only explain the main points of this method. First, the nonlinear integral equation (7) is reduced to a sequence of Fredholm integral equations of the second kind, which can be solved successively by means of a Newtonian iterative procedure. Then we use multiknot cardinal spine functions to make kernels of the integral equation become Fredholm integral equations of the second kind with degenerated kernels. Then the problem to solve a system of simultaneous linear algebraic equations is completed by the Gauss elimination method. This program can be carried out by the following procedure. For a given geometry, boundary condition coefficients, and physical constants, p is chosen to be sufficiently small so that the linear solution [obtained by neglecting nonlinear terms in Eq. (7)] is adequate. Taking it as the initial step for the iteration process, we can get a nonlinear

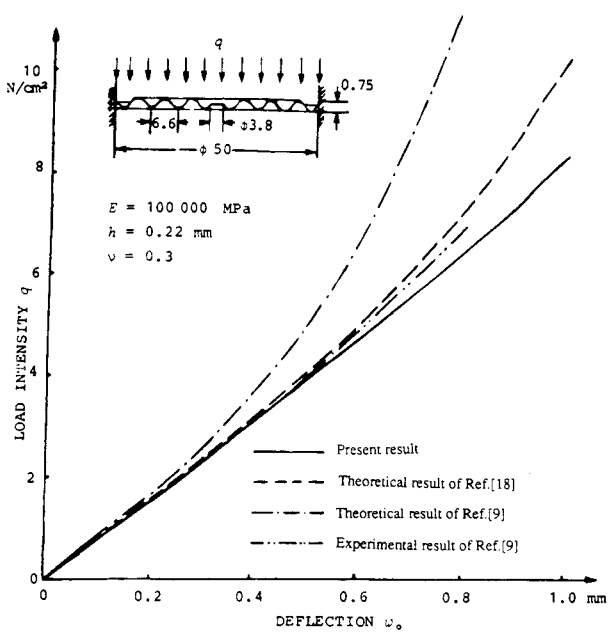

Fig. 2 Comparison between analytical predictions and experimental results for a rigidly clamped circular corrugated diaphragm.

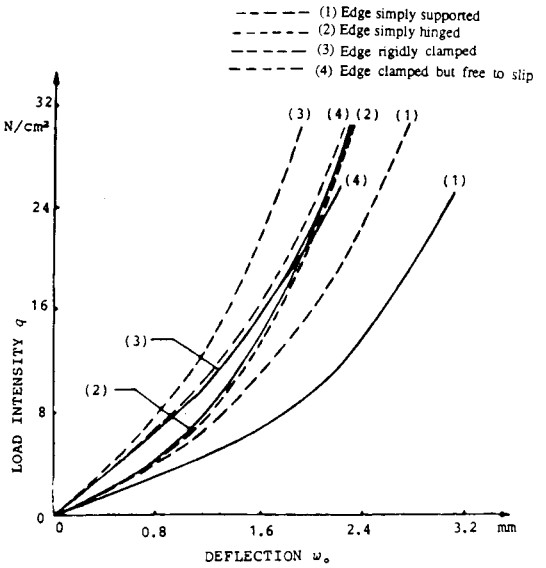

Fig. 3 Curves of elastic characteristics for boundary conditions (1-4).

solution corresponding to this p value. Then we may give a positive or negative increment of p and use the convergent solution of the previous p as an initial value for the interation process of the new p value. By this procedure, we can get the required solution for the prebuckling or the postbuckling states corresponding to any value p of the load.

In carrying out the calculation, a convergent criterion of 0.001% maximum error is adopted. As the method discussed in this paper has a quadratic rate of convergence, this condition can be satisfied, requiring only four or five iterations in most cases.

III. Method of Solution and Computational Techniques

Defining an operator F as follows

$$y = F(\alpha)$$

$$y(x) = \alpha(x) + pf(x) + \int_0^1\int_0^1 G_1(x,s)\, G_2(s,t)\, [\alpha(s) + I(s - x^*)\lambda \sin(\omega s + \phi)]\, [\tfrac{1}{2}\alpha(t)^2 + I(t - x^*)\lambda \sin(\omega t + \phi)\alpha(t)]\, ds\, dt \qquad (11)$$

in the normalized linear space $C[0, 1]$ and applying the Newtonian iterative procedure

$$F'(\alpha_n)(\Delta\alpha_n) = -F(\alpha_n)$$

$$\Delta\alpha_n = \alpha_{n+1} - \alpha_n \qquad (n = 0, 1, \ldots) \qquad (12)$$

to the operator equation $F(\alpha) = 0$, a sequence of Fredholm integral equations of the second kind are obtained

$$\alpha_{n+1} - \int_0^1 G_n^*(x,s)\alpha_{n+1}(s)\, ds = F_n(x)$$

$$(0 \le x \le 1,\ n = 0, 1, 2, \ldots) \qquad (13)$$

where the kernel $G_n^*(x,s)$ and nonhomogeneous term $F_n(x)$ are determined by the last degree iteration and are continuous in the respective domains of definition. Then, we obtain a uniform approximation for the kernel G_n^* and the nonhomogeneous term F_n by multiknot cardinal spline functions as follows:

$$\tilde{G}_n(x,s) = \sum_{i,j} G_{n,ij} \overset{N}{\Phi}_i(x) \overset{M}{\Phi}_j(s), \qquad \tilde{F}_n(x) = \sum_i F_{n,i} \overset{N}{\Phi}_i(x) \qquad (14)$$

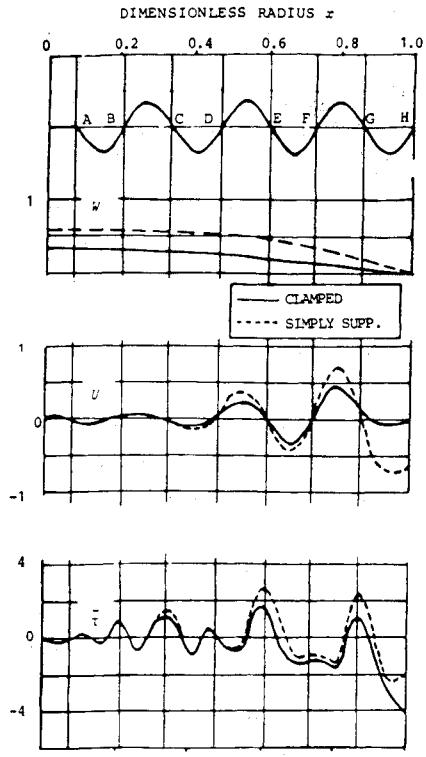

Fig. 4 Dimensionless deflection, radial displacement, and shearing stress.

so that Eq. (13) may be approximately replaced by a sequence of Fredholm integral equations of the second kind with degenerated kernels

$$\alpha_{n+1}(x) - \int_0^1 \bar{G}_n(x,s)\alpha_{n+1}(s)\,ds = \bar{F}_n(x)$$

$$(0 \le x \le 1,\ n = 0, 1, 2, \ldots) \tag{15}$$

As a result, a solution of Eq. (15), i.e., an approximate solution of Eq. (13), is obtained

$$\alpha_{n+1}(x) = \sum_{i=0}^{N} C_i^{(n+1)} \overset{N}{\Phi}_i(x) \tag{16}$$

where $C_i^{(n+1)} = \alpha_{n+1}(x_i)$ for $i = 0, 1, \ldots, N$, and are determined by a system of linear algebric equations

$$C_i^{(n+1)} - \sum_{k=0}^{N} C_k^{(n+1)} a_{ik}^{(n)} = F_{n,i}$$

$$(i = 0, 1, \ldots, N;\ n = 0, 1, 2, \ldots) \tag{17}$$

In the above,

$$a_{jk}^{(n)} = \sum_{j=0}^{M} G_{n,ij}^{*}\, b_{jk} \qquad (i, k = 0, 1, \ldots, N) \tag{18}$$

$$b_{jk} = \int_0^1 \overset{M}{\Phi}_j(s)\, \overset{N}{\Phi}_k(s)\,ds$$

$$(j = 0, 1, \ldots, M;\ k = 0, 1, \ldots, N) \tag{19}$$

$G_{n,ij}^{*}$ and $F_{n,i}$ are values of the functions G_n^{*} and F_n, respectively, at the nodal points (x_i, s_j) and (x_i) on the uniform meshes

$$\{(x_i, s_j)\},\ \{x_i\};\ x_i = (i/N),\ s_j = (j/M)$$

$$(i = 0, 1, \ldots, N;\ j = 0, 1, 2, \ldots, M)$$

The expressions $\overset{N}{\Phi}_i(x)$ and $\overset{M}{\Phi}_j(s)$ are multiknot cardinal spline functions[23] with degree not less than 3. The integers N and M denote total numbers of equal intervals that are divided from $0 \le x \le 1$ and $0 \le s \le 1$, respectively. The integrals of Eq. (19) can be obtained in simple closed form, and few b_{jk} need to be calculated, most of them being zero according to the local nonzero character of the multiknot cardinal spines. Correspondingly, the terms that take part in summing up in Eq. (18) are few.

Eventually, solving successively Eq. (13) by an efficient Gaussian elimination scheme and substituting the $[C_i^{(n+1)}]$ into Eq. (16), the desired solution of Eq. (7), which fulfills the requiring precision, may be obtained if the mesh spacing is sufficiently small and the iterations converge.

The convergence theorem of the previously mentioned iteration procedure has been given in Ref. 24. In the numerical analysis, the following numerical criterion for convergence is employed

$$\epsilon_n \equiv \max_i \{\,|\alpha_{n+1}(x_i) - \alpha_n(x_i)|\,\} < 10^{-4} \tag{20}$$

Test calculations were made with 10^{-8} instead of 10^{-4}. The replacement had no significant effect. In all cases, except in the vicinity of critical points, solutions that fulfill condition (20) can be obtained after four or five iterations due to the quadratic rate of convergence of the Newtonian iterative procedure.

The numerical procedure just described is started as follows. For any given values of all of the parameters except p, the latter is chosen sufficiently small that the linear solution [obtained by suppressing nonlinear terms in Eq. (7)] is adequate. With this as a starting solution, one may obtain the desired nonlinear solution, written as $\alpha(x, p)$, corresponding to the value of p by the earlier iterations. Having the solution $\alpha(x, P)$ for any load parameter p, the initial iteration for a load parameter $p + \Delta p$ is taken as $\alpha_0(x, P + \Delta p) = \alpha(x, p)$ and the iterations are performed. It is observed that the number of iterations required for convergence increases as $p \to p_c$ (i.e., the buckling load) from below—i.e., on the unbuckled branch.

Following this procedure, we use as an initial iteration an unbuckled solution and have no difficulty obtaining a buckled solution for $p = p + \Delta p$, provided Δp is not too small. The

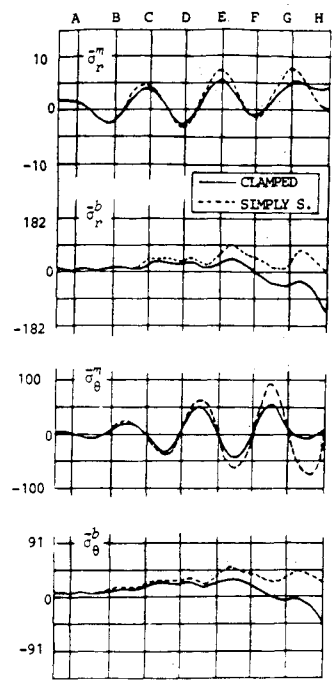

Fig. 5 Dimensionless membrane stress and bending stress components.

solution thus jumps from the unbuckled to the buckled state when p_c is exceeded. Once buckling has been observed, which is obvious from the large changes in the solution—i.e., a jump in the deflection—we employ $\alpha(x, p)$ on the buckled branch as a starting iteration and proceed as before, now obtaining buckled solutions for increasing and decreasing values of the load about p_c. As $p \to p_b$, the buckled solutions require more iterations for convergence. When the load is finally reduced to $p = p_b - \Delta p$, below the lower buckling load, the solution jumps back to a previously obtained solution. Thus, for the interval $p_b < p < p_c$, we obtain two or more distinct sets of solutions of the system of algebraic equations (17), no doubt corresponding to the pair of nonunique solutions of the boundary-value problem.

The numerically determined upper buckling load p_c is defined to lie in the interval

$$\bar{p} \leq p_c \leq \bar{p} + \Delta p \tag{21}$$

if an unbuckled solution has been obtained for $p = \bar{p}$, and using the solution as the initial iteration, a buckled solution is obtained for $p = \bar{p} + \Delta p$. The lower buckling load is located in a similar manner. For these determinations we use Δp as small as possible until we have located p_c and p_b to a satisfactory accuracy.

IV. Discussion of Solutions

Here we adopt multiknot cardinal spline functions of third degree to carry out numerical calculations in the case of $\nu = 0.3$ for two kinds of corrugated diaphragms. The mesh spacing is chosen as $\Delta x = \Delta s = \Delta t = 0.016666$, and the results obtained are given in Figs. 2-9, of which Figs. 4-9 are in dimensionless form.

Figure 2 gives characteristic load vs central deflection curves for the circular corrugated diaphragm with edge rigidly clamped. The results coincide very nearly with experimental results in Ref. 9 and analytic ones in Ref. 18 as $w_o/h \leq 2.5$. Our results are closer to those in Ref. 9 than those in Ref. 18. As load increases, theoretical results in Refs. 18 and 9 move away from the experimental results in Ref. 9 toward lower deflections, but our results move toward higher deflection and almost coincide with the results reported in Ref. 16, which were obtained by orthotropic plate theory. Figure 3 gives the characteristic curve of the corrugated diaphragm of Fig. 2 with four different boundary conditions (1-4), in which solid lines represent the response to pressure from above, and dotted lines represent the response to pressure from below the diaphragm. The solid line and dotted line corresponding to the same edge condition are different. This means there is a difference in the elastic response and such difference becomes larger for larger deflections. It is impossible for the orthotropic plate theory to identify such characteristics. We also see that the corrugated diaphragm is more flexible in the case of a simply supported edge and more rigid in the case of a rigidly clamped edge.

Figures 4-7 give the displacements and stresses of the corrugated diaphragm of Fig. 1 in cases of a rigidly clamped edge and a simply supported edge in dimensionless form, with $p = 500$. The dimensionless deflection and radial displacement are defined as the following:

$$W = \sqrt{12(1 - \nu^2)}\,(w/h) \tag{22a}$$

$$U = 12r_1(1 - \nu^2)\,(u/h^2) \tag{22b}$$

They are plotted in Fig. 4. It is easy to see that the corrugated diaphragm in the case of a simply supported edge is slightly more flexible than that in the case of a rigidly clamped edge. But for radial displacements, near the outer edge, there is an obvious difference between these two cases. Besides, the variation of U exhibits a pattern at the same wave frequency as the number of corrugations.

We define the dimensionless quantities of local normal stress and shearing stress as follows:

$$\bar{\sigma} = \frac{12(1 - \nu^2)r_1^2}{Eh^2}\,\sigma \tag{23a}$$

$$\bar{\tau} = \frac{12(1 - \nu^2)r_1^2}{Eh^2}\,\tau \tag{23b}$$

According to the theory of thin shells, the normal stress is a small quantity that can be neglected. The shearing stresses have a parabolic distribution along the thickness and vanish on the upper and lower surfaces. They have a maximum value τ at the neutral surface ($z = 0$) of the shell that is related to the shearing force Q_r by the expression

$$\tau = 3Q_r/2h \tag{24}$$

This stress is plotted in Fig. 4 in dimensionless form, in which there is a noticeable difference in the curves for a rigidly clamped edge and a simply supported edge near the edge. The shearing stress varies with double frequency and has a maxi-

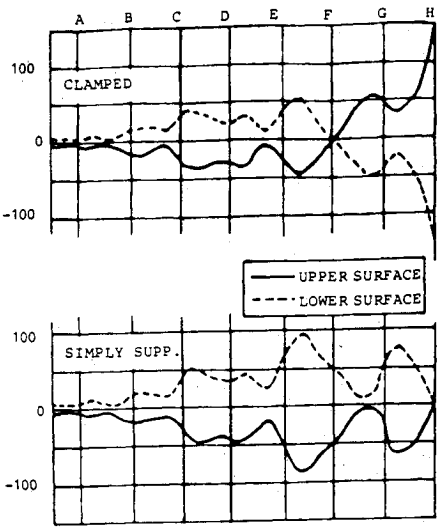

Fig. 6 Total dimensionless radial stress at upper and lower surfaces.

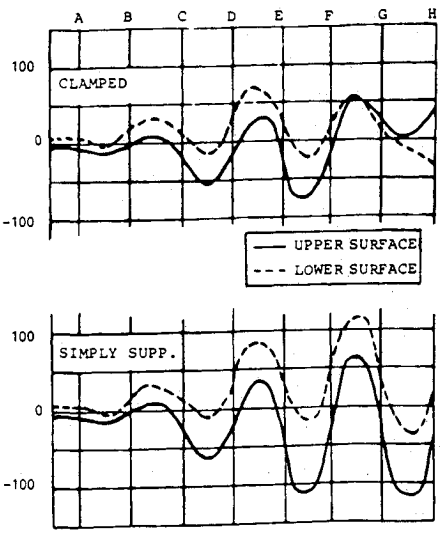

Fig. 7 Total dimensionless circumferential stress at upper and lower surfaces.

mum positive value at $r = 0.6r_1$ and a minimum in the neighborhood of the outer edge. In comparison with other stress components given later, the shearing stress is very small and can be neglected.

Membrane stresses σ_r^m and σ_θ^m are uniformly distributed along the thickness of the shell. They have the following relations with membrane forces:

$$\sigma_r^m = N_r/h \tag{25a}$$

$$\sigma_\theta^m = N_\theta/h \tag{25b}$$

Bending stresses σ_r^b and σ_θ^b are linear functions of the coordinate z along the thickness and have the maximum and minimum values on the upper and lower surfaces of the corrugated diaphragm. Bending stresses have the following relations with the bending moments:

$$\sigma_r^b(\pm h/2) = \pm 6M_r/h^2 \tag{26a}$$

$$\sigma_\theta^b(\pm h/2) = \pm 6M_\theta/h^2 \tag{26b}$$

The positive sign corresponds to lower surfaces and the negative sign to upper surfaces when the loading is from above.

In cases of a rigidly clamped edge and a simply supported edge, Fig. 5 gives, in order, radial membrane stress, radial bending stress on the lower surface, circumferential membrane stress, and circumferential bending stress on the lower surface in dimensionless form, i.e., $\bar{\sigma}_r^m$, $\bar{\sigma}_r^b$, $\bar{\sigma}_\theta^m$, and $\bar{\sigma}_\theta^b$ according to definition (23a). It should be pointed out that, although the results obtained in the interior region of the corrugated diaphragm in cases of a rigidly clamped edge and a simply supported edge are different throughout, it is only in a narrow region near the outer edge where this difference becomes noticeable.

The top graph of Fig. 5 shows that the radial membrane stress is very small, so that we had to enlarge the scale of the ordinate to make it distinguishable. The top and the second graph of Fig. 5 indicate that the radial bending stress $\bar{\sigma}_r^b$ is much larger than the radial membrane stress $\bar{\sigma}_r^m$. In comparing the two, the latter can be neglected. The lower two graphs of Fig. 5 represent circumferential bending stress $\bar{\sigma}_\theta^b$ and circumferential membrane stress $\bar{\sigma}_\theta^m$, whose magnitudes are of the same order.

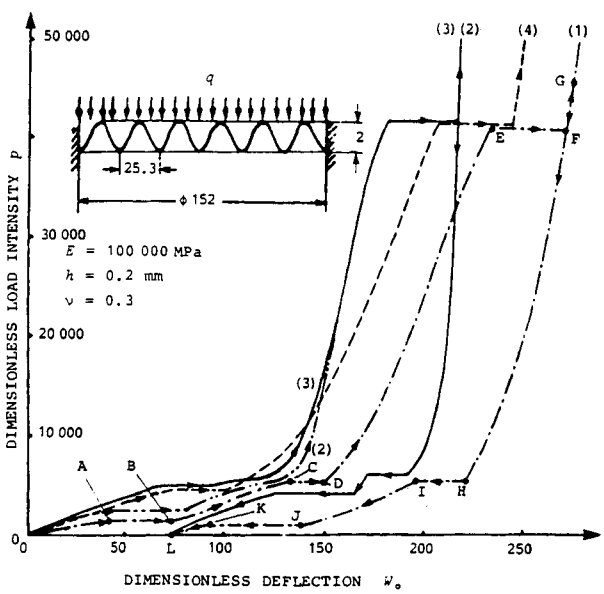

Fig. 8 Curves of loading and unloading processes with snap throughs and snap backs.

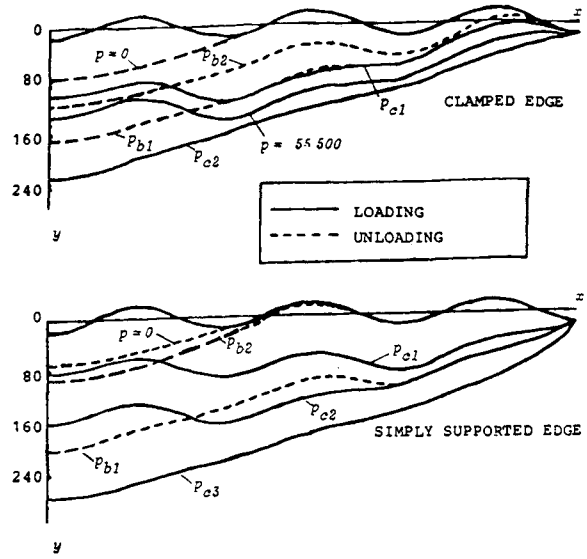

Fig. 9 Original and post buckling cross sections of diaphragm under two different edge support.

Among the previously mentioned four stress components, membrane stresses exhibit the same wave frequency as the corrugated shape; bending stresses exhibit double frequency.

The total stress components in the lower (plus) and upper (minus) surfaces are as follows:

$$\sigma_r(\pm h/2) = \sigma_r^m \pm \sigma_r^b(h/2) \tag{27a}$$

$$\sigma_\theta(\pm h/2) = \sigma_\theta^m \pm \sigma_\theta^b(h/2) \tag{27b}$$

Figures 6 and 7 give the total radial and circumferential stresses on the upper and lower surfaces for a rigidly clamped edge and a simply supported edge in dimensionless form.

Figure 8 gives the elastic characteristic curves of the loading process of the corrugated diaphragm with three sine-shaped waves under four kinds of boundary conditions, as previously expressed, and the unloading process characteristic curves under the boundary conditions of a rigidly clamped edge (case 3) and a simply supported edge (case 1). It is not difficult to see that, as the load is continuously increased or decreased, the routes of these two processes are different. In the curves of the loading process appear two or three discontinuities (snap throughs) and in the unloading process there appear two or one discontinuities (snap backs). As a matter of fact whether the edge is rigidly clamped or simply supported, the unloading curve of the diaphragm, after all of the wave peaks disappear, intersects the abscissa almost at the same point L, and does not return to the origin of the coordinate system, which signifies that, even though the whole load has vanished after all of the wave peaks of the corrugation disappear, the corrugated diaphragm cannot recover to its original shape. This case is similar to the snap through of a spherical cap with a negative snap-back load, which is well known, where even if the load has been moved away from the buckled cap, the cap does not return to its original shape but maintains a residual deflection due to the stored energy. Taking case 1 of a simply supported edge as an example, the loading curve has three discontinuities: the p values at these discontinuities represent the first, second, and third snap-through loads p_{c1}, p_{c2}, and p_{c3} ($p_{c1} < p_{c2} < p_{c3}$), respectively, and the unloading curve has two snap-back loads p_{b1} and p_{b2} ($p_{b1} > p_{b2}$). The route of the loading process is O-A-B-C-D-E-F-G with snap through at load p_{c1} between A and B, snap through at load p_{c2} between C and D, and snap through at load p_{c3} between E and F. The route of the unloading process is G-F-H-I-J-K-L, with snap back at load p_{b1} between H and I, and snap back at load p_{b2} between J and K, and eventual intersection of the abscissa at point L.

Figure 9 represents the shape of the initial axial cross section of the corrugated diaphragm and the shape of axial cross section including the results of the discontinuities of the characteristic curve of Fig. 8 under a simply supported edge and a rigidly clamped edge [$Y \equiv \sqrt{12(1-\nu^2)}\,(w + w_I)/h$], in which solid lines and dotted lines correspond to results of the loading and unloading processes, respectively. From the upper part of the figure, we see that, for the case of a simply supported edge, as the load increases gradually from zero to the first snap-through load p_{c1}, the wave near the outer edge begins to snap, then as the load increases to p_{c2}, the next wave snaps, and then the load decreases to p_{c3}, the wave near the center of the corrugated diaphragm snaps and provides the final instability. At this time, the axial cross section of the corrugated diaphragm becomes rather flat (i.e., the curvature of the meridian line is very small everywhere), and afterward, the rigidity of the corrugated diaphragm rises sharply (see Fig. 8). From now on, as the load increases further, there is no more snapping of the corrugated diaphragm. If after this we unload gradually and the load decreases to p_{b1}, the diaphragm experiences the first snap back and the second wave jumps back. As the load decreases to p_{b2}, the wave near the outer edge of the corrugated diaphragm jumps back. After this, the load decreases continuously until all of the load is released ($p = 0$) and we see from the figure that the wave near the center has not snapped back. The central deflection of the corrugated diaphragm is and remains at point L in Fig. 8.

The snap-through and snap-back processes are different in the case of a rigidly clamped edge. Because of the edge condition, the wave that experiences the first snap through is not the first one near the outer edge, but the second one. As the load continues to increase, the peak of the wave near the outer edge gradually disappears but no snap through occurs. Therefore, on the loading curve in the case of the rigidly clamped edge, there are only two discontinuities. If, after this, we begin to unload gradually, two snap backs will occur, but as the diaphragm is completely unloaded ($p = 0$), the wave of the corrugated diaphragm near the center has not snapped back.

From the figure, we see that, no matter whether the edge is rigidly clamped or simply supported, the wave near the center does not snap back, unlike the two waves near the outer edge, which return to the initial position they had prior to buckling. Therefore, the edge condition has only a small influence on the central deflection, and thus, curves of the unloading process in cases of a rigidly clamped edge and of a simply supported edge intersect with the abscissa at almost the same point L.

V. Conclusions

1) Elastic response are different for loads acting in opposite directions on the diaphragm. The larger the deflection is, the greater the difference is.

2) The transverse shearing stress τ and the radial membrane stress σ_r^m are negligibly small when compared with the other stress components.

3) The distribution of stress and displacement in a corrugated diaphragm exhibits the same oscillating behavior as the wave shape of the diaphragm.

4) The loss of stability, i.e., the buckling of a corrugated diaphragm is a phenomenon consisting of a series of local instabilities of the individual waves. When the number of waves is large, the number of wave snap throughs is also large. The total number of snap throughs is, however, never greater than the number of waves.

5) When buckling has occurred, the loading and unloading processes may have different characteristics. i.e., the elastic behavior of the diaphragm in the unloading process after m snap throughs and n snap backs ($m \geq n$) may be completely different from elastic behavior during the loading process.

6) After buckling, and subsequent complex unloading, certain waves may not return to their initial prebuckling state.

This paper provides a theoretical foundation for the extension of the use of corrugated diaphragms into control elements, and its results can be adapted directly as design data for engineering use. As far as we know, the corrugated diaphragm has not yet been used as a control element.

Acknowledgments

The first two authors were supported by the Fund for Doctor Centers of the National Educational Committee, People's Republic of China.

References

[1]Hersey, M. D., "Diaphragms of Aeronautic Instruments," NACA TR 165, 1923.

[2]Griffith, A. A., "The Theory of Pressure Capsules," British Aeronautical Research Council, R&M 1136, 1928.

[3]Panov, D. U., "Large Deflection of Circular Diaphragms with Shallow Corrugation," *Applied Mathematics and Mechanics,* Vol. 5, No. 2, 1941, p. 203, (in Russian).

[4]Haringx, J. A., "The Rigidity of Corrugated Diaphragms," *Applied Scientific Research,* Vol. 2, Series A, The Netherlands, 1950.

[5]Eck, B., "Charakteristische Eigenschaften von Membranblechen für Regelvorrichtungen and Instrumente," ZAMM, Bd. 7, 1927.

[6]Wildhack, W. A., Goerke, V. H., "Corrugated Metal Diaphragms for Aircraft Pressure-Measuring Instruments," NACA TN 738, 1939.

[7]Feodoseev, V. I., "Precise Instrumental Structures," Defence Press, Moscow, 1949.

[8]Volmir, A. S., "Flexible Plates and Shells," Technical Press, Moscow, 1956.

[9]Andreeva, L. E., "Corrugated Diaphragms Treated as Anisotropic Plates," *Engineering Collected Works,* Vol. 21, 1955 (in Russian).

[10]Akasa, T., "On the Elastic Properties of the Corrugated Diaphragm," *Journal of the Japan Society for Aeronautical & Space Sciences,* Vol. 3, No. 22, 1955.

[11]Yokoi, R., "A Theorical Analysis on the Linear Maximmum Deflection of Corrugated Metallic Diaphragm Capsules," TSICE, Vol. 15, No. 5, 1969.

[12]Yokoi, R., "Non-linear Maximum Deflection of Corrugated Metallic Capsules," *Journal of the Japan Society of Precision Engineering,* Vol. 37, No. 3, 1971.

[13]Yokoi, R., "An Analysis of Maximum Deflection on Corrugated Metallic Diaphragm Capsule, Effect of Control Rigid Body on the Deflection, etc.," *Journal of the Japan Society of Precision Engineering,* Vol. 37, No. 11, 1971.

[14]Andreeva, L. E., *Elastic Elements of Instruments,* Machine Manufacture Press, 1962.

[15]Liu, R-h., "The Characteristic Relations of Corrugated Circular Plates," *Acta Mechanica Sinica,* Vol. 1, 1978, pp. 47–52 (in Chinese).

[16]Chen, S-l., "Elastic Behaviour of Uniformly Loaded Circular Corrugated Plate with Sine-Shaped Shallow Waves in Large Deflection," *Applied Mathematics and Mechanics,* Vol. 1, No. 2, 1980, pp. 279–291.

[17]Wang, X-z., "Large Deflection Behaviour of Uniformly Loaded Circular Corrugated Plate," *Journal of Gansu University of Technology,* Vol. 2, 1981 (in Chinese).

[18]Liu, R-h., "Nonlinear Bending of Corrugated Annular Plates," *Scientia Sinica, Series A,* Vol. 3, 1984.

[19]Liu, R-h,, "Large Deflection of Corrugated Circular Plate with Plane Boundary Region," *SM Archives,* No. 9, 1984.

[20]Thurston, G. A., "A New Method for Computing Axisymmetric Buckling of Spherical Caps," *Journal of Applied Mechanics,* Vol. 38, 1871, pp. 179–184.

[21]Kaplan, A., "Buckling of Spherical Shells, Thin-Shell Structures—Theory, Experiment, and Design," edited by Y. C. Fung and E. E. Sechler, Prentice-Hall, Englewood Cliffs, NJ, 1974, pp. 274–288.

[22]Mescall, J. F., "Numerical Solutions of Nonlinear Equations for Shells of Revolution," *AIAA Journal,* Vol. 4, 1966, pp. 2041–2043.

[23]Ueshen, L., and Tongshu, Q., *Spline Function Methods,* Science Press, Beijing, PRC, 1979, pp. 110–114.

[24]Song, W-p., "Newton-Spline Method in the Nonlinear Theory of Shells of Revolution," *Chinese Science Bulletin,* Vol. 34, No. 3, 1989, pp. 193–198.

[25]Yeh, K-y., and Song, W-p., "Axisymmetrical Buckling of the Shallow Circular Spherical Shell under the Action of Uniform Pressure," *Journal of Lanzhou University (Natural Sciences),* Vol. 23, No. 2, 1987, pp. 18–27 (in Chinese).